Acta Oceanol. Sin., 2024, Vol. 43, No. 5, P. 54–64
https://doi.org/10.1007/s13131-024-2324-9
http://www.aosocean.com
E-mail: ocean2@hyxb.org.cn

Study of the ability of SWOT to detect sea surface height changes caused by internal solitary waves

Hao Zhang[1, 2, 3], Chenqing Fan[1, 2, 3], Lina Sun[1, 2], Junmin Meng[1, 2*]

[1] First Institute of Oceanography, Ministry of Natural Resources, Qingdao 266061, China

[2] Technology Innovation Center for Ocean Telemetry, Ministry of Natural Resources, Qingdao 266061, China

[3] College of Oceanography and Space Informatics, China University of Petroleum (Huadong), Qingdao 266580, China

Received 12 December 2023; accepted 15 March 2024

Abstract

Surface Water and Ocean Topography (SWOT) is a next-generation radar altimeter that offers high resolution, wide swath, imaging capabilities. It has provided free public data worldwide since December 2023. This paper aims to preliminarily analyze the detection capabilities of the Ka-band radar interferometer (KaRIn) and Nadir altimeter (NALT), which are carried out by SWOT for internal solitary waves (ISWs), and to gather other remote sensing images to validate SWOT observations. KaRIn effectively detects ISW surface features and generates surface height variation maps reflecting the modulations induced by ISWs. However, its swath width does not completely cover the entire wave packet, and the resolution of L2/L3 level products (about 2 km) cannot be used to identify ISWs with smaller wavelengths. Additionally, significant wave height (SWH) images exhibit blocky structures that are not suitable for ISW studies; sea surface height anomaly (SSHA) images display systematic left-right banding. We optimize this imbalance using detrending methods; however, more precise treatment should commence with L1-level data. Quantitative analysis based on L3-level SSHA data indicates that the average SSHA variation induced by ISWs ranges from 10 cm to 20 cm. NALTs disturbed by ISWs record unusually elevated SWH and SSHA values, rendering the data unsuitable for analysis and necessitating targeted corrections in future retracking algorithms. For the normalized radar cross section, Ku-band and four-parameter maximum likelihood estimation retracking demonstrated greater sensitivity to minor changes in the sea surface, making them more suitable for ISW detection. In conclusion, SWOT demonstrates outstanding capabilities in ISW detection, significantly advancing research on the modulation of the sea surface by ISWs and remote sensing imaging mechanisms.

Key words: internal solitary waves, Surface Water and Ocean Topography (SWOT), Ka-band radar interferometer (KaRIn), Nadir altimeter (NALT), sea surface height anomaly (SSHA), normalized radar cross section (NRCS)

Citation: Zhang Hao, Fan Chenqing, Sun Lina, Meng Junmin. 2024. Study of the ability of SWOT to detect sea surface height changes caused by internal solitary waves. Acta Oceanologica Sinica, 43(5): 54–64, doi: 10.1007/s13131-024-2324-9

1 Introduction

Internal solitary waves (ISWs), a type of gravity wave that occurs at the interface of stratified fluid systems, have been observed in many sea areas and large lakes worldwide (Gerkema and Zimmerman, 2008). ISWs are important hydrodynamic phenomena with large amplitudes, short periods, and fast velocities (Huang et al., 2016). ISWs play an important role in biological primary production and the evolution of the climatic environment, with considerable implications for global marine ecosystems and ocean engineering. Near the continental shelf, nutrients in deep seawater can be transported to the surface layer, where they foster the growth of coral reefs (Wang et al., 2007; Liu et al., 2022), fish and other creatures (Bondur et al., 2020; Moore and Lien, 2007; Pineda et al., 2020); moreover, ISWs can also harm submarines (Gong et al., 2022), drilling platforms (Jackson et al., 2013), and oil pipelines (Bole et al., 1994).

Although ISWs originate near the underwater density thermocline interface, their propagation significantly modulates surface features. They induce a redistribution of small-scale waves, leading to convergence and divergence of particles (Alpers, 1985), which visually manifests as alternating bright and dark stripes in Synthetic Aperture Radar (SAR) and optical images. Furthermore, ISWs cause vertical undulations in sea surface structures (Magalhães and da Silva, 2017), a phenomenon that has been confirmed through field observations and laboratory experiments (Fig. 1). However, the changes in sea surface height (SSH) induced by these waves are not reflected in SAR or optical imagery; the introduction of radar altimetry addresses this issue (Stammer, 1997; Le Traon et al., 1998). With advancements in altimeter detection precision, precise centimeter-level measurements of SSH have become achievable.

Altimeters primarily measure the distance from satellites to the sea surface nadir point, and their evolution includes three generations. The first generation comprises traditional radar altimeters (RAs), represented by the Topography Experiment (TOPEX) and Jason series (Nerem et al., 2010). The second generation features synthetic aperture radar altimeters (SRALs), exemplified by Sentinel-3 and Sentinel-6 (Donlon et al., 2012; Ray et al., 2015). The third generation encompasses three-dimensional imaging radar altimeters. In comparison to the former two

Foundation item: The National Natural Science Foundation of China under contract Nos U2006207 and 42006164.
*Corresponding author, E-mail: mengjm@fio.org.cn

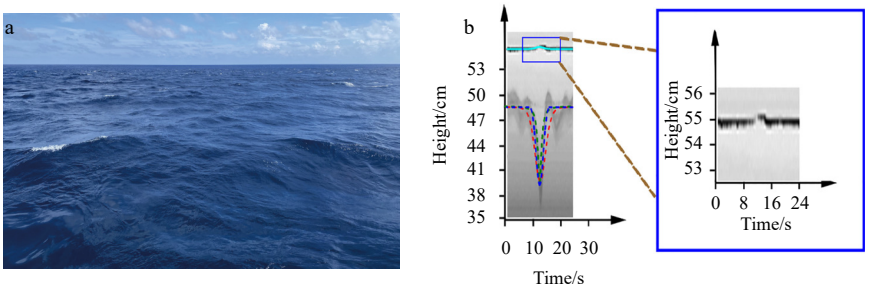

Fig. 1. Sea surface height variations caused by internal solitary waves (ISWs). a. Field image of changes in the sea surface upon the arrival of ISWs; b. laboratory experimental image (Zhang et al., 2022).

generations, imaging radar altimeters integrate existing altimetry techniques, synthetic aperture technology, and interferometric measurements, offering advantages such as high resolution, wide swath coverage, and imaging capability. The currently available imaging altimeters include the Ku-band interferometric imaging radar altimeter (InIRA), which was constructed by China's Tiangong-2 Space Laboratory (Zhang et al., 2000, 2018a; Dong et al., 2017), and the Ka-band radar interferometer (KaRIn), which was developed jointly by the United States and France and was mounted on the Surface Water and Ocean Topography (SWOT) project (Durand et al., 2010; Fu et al., 2009).

Many studies have utilized altimeters to investigate ISWs. In the domain of RAs, analyses of the modulation patterns of altimeter signals due to ISWs have been conducted based on Jason-2 data (Magalhães and da Silva, 2017; da Silva and Cerqueira, 2016; Zhang et al., 2018b). Concerning SRALs, studies have primarily employed Sentinel-3 and Sentinel-6 data. These investigations include an analysis of the modulatory effects of ISWs on SRAL geophysical parameters (Santos-Ferreira et al., 2018; Yu et al., 2022), a quantitative assessment of SSH variations induced by ISWs (Zhang et al., 2020), an estimation of the amplitude and velocity of ISWs using SRAL data (Santos-Ferreira and da Silva, 2020), and the development of automatic detection algorithms for ISWs using SRAL data (da Silva et al., 2020). Using imaging altimetry, Zhang et al. preliminarily analyzed the feasibility of capturing the two-dimensional sea surface characteristics of ISWs and the information regarding sea surface vertical undulations using InIRA. Their study demonstrated the potential of three-dimensional imaging altimetry for detecting ISWs (Zhang et al., 2022). However, due to limitations in the data volume and measurement precision of the InIRA, this study did not fully reveal the regularities in SSH changes induced by ISWs.

Overall, SWOT has broader prospects for studying SSH changes induced by ISWs. Launched on December 16, 2022, SWOT primarily utilizes SAR radar interferometry for high-resolution two-dimensional height field observations of global oceanic and terrestrial hydrology. While traditional altimeters can observe oceanic dynamic phenomena at a resolution of 100 km, SWOT can describe mesoscale and submesoscale phenomena within a spatial resolution of 15 km or greater (Biancamaria et al., 2016; Fu and Ubelmann, 2014; Morrow et al., 2019). This capability extends to the formation, evolution, and dissipation of ISWs and their modulation effects on the sea surface, which are the focus of this paper. Furthermore, the wide swath coverage of SWOT allows KaRIn to acquire observation swaths of approximately 50 km on each side, with a center gap of +/–10 km filled by the dual-frequency Nadir altimeter (NALT). This approach significantly expands the observational range of altimetry for studying oceanic phenomena.

Previously, scholars have conducted studies on the detection capabilities of SWOT for oceanic phenomena, such as eddies and currents, based on simulations and theoretical computations (Armitage and Kwok, 2021; Chaudhary et al., 2021; Ma and Han, 2019; Yu et al., 2021). However, there is currently no publicly available literature regarding the performance of SWOT in detecting ISWs. Can the NALT and KaRIn onboard SWOT collaboratively observe ISWs? Will the SSH changes induced by ISWs be notably represented in KaRIn? These questions have sparked our research interest.

Therefore, the primary focus of this manuscript includes the preprocessing of SWOT NALT and KaRIn data and the quantitative analysis of SSH changes induced by ISWs. Additionally, we aim to identify the strengths and limitations of SWOT in detecting ISWs. This research endeavors not only to advance the finer study of sea surface features related to ISWs but also to expand the applications of three-dimensional imaging altimetry.

2 Data

SWOT operates at an orbit altitude of 890.5 km and an inclination angle of 77.6°. Utilizing a nonsynchronous orbit, it has a revisit cycle of 20.86 d, comprising a total of 584 passes per cycle. The primary payload instruments used include a NALT with dual frequency, a KaRIn operating at 35.75 GHz, a three-frequency microwave radiometer (RAD), and a precise orbit determination (POD) system.

2.1 *KaRIn*

KaRIn is a Ka-band dual-swath observation system. By employing the SAR interferometry technique, the swaths on both sides of the nadir track are alternately illuminated. Ultimately, two-dimensional height field images are detected and generated on two 50 km-wide swaths with a 20 km separation (Fig. 2a). The left and right swaths of KaRIn operate under H-polarization and V-polarization, respectively (Fig. 2b).

The data of interest for open ocean regions are termed low-resolution (LR) data, which undergo preprocessing on a satellite and achieve an average altimetric accuracy of more than 0.5 cm. The Level-2 (L2) data distributed by KaRIn primarily include four types, as outlined in Table 1. In January 2024, NASA provided Level-3 (L3) data (https:// swot.jpl.nasa.gov/), which corrects the L2 data and includes basic and expert files, available in the SSH and sea surface height anomaly (SSHA).

2.2 *NALT*

NALT is a Poseidon-3C that operates in the C-band (5.3 GHz) and Ku-band (13.58 GHz). NALT collects data in the gap between the KaRIn swaths, obtaining the normalized radar cross section (NRCS), SSH, SSHA, and significant wave height (SWH) in the

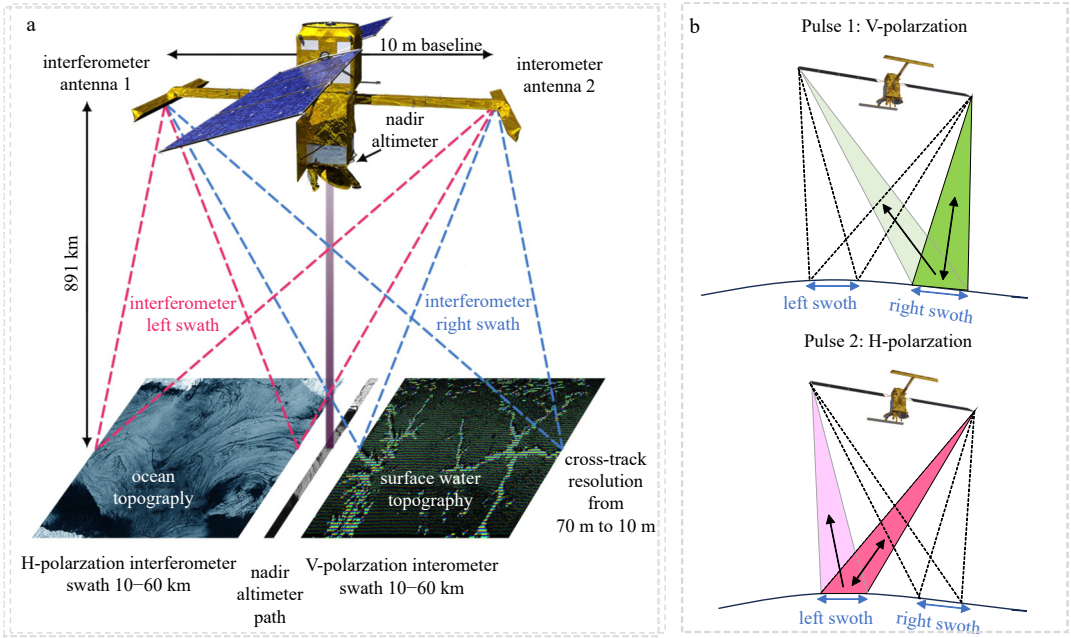

Fig. 2. Schematic diagram illustrating the operation of Surface Water and Ocean Topography (a) and polarization modes of the two antennas (b).

Table 1. Ka-band radar interferometer Level 2 data

Data type	Grid	Key data variables	Other
Basic	2 km	SSH, SSHA	sea surface height (SSH), sea surface height anomaly (SSHA)
WindWave	2 km	SWH, NRCS	significant wave height (SWH), normalized radar cross section (NRCS)
Expert	2 km	SSH, SSHA, SWH, NRCS	all variables contained within the Basic and WindWave files, along with additional variables used for detailed data analysis and processing
Unsmoothed	250 m	SSH, NRCS	without additional smoothing, split into left and right swaths

nadir direction. The publicly available NALT data include L2 Operational Geophysical Data Record (OGDR), Interim Geophysical Data Record (IGDR), and Geophysical Data Records (GDR) data, which are distributed at 1 Hz and 20 Hz. Table 2 lists the IGDR data parameters used in the analysis conducted in this paper.

The generation and propagation characteristics of ISWs are primarily determined by tidal and topographical factors. The spatial features of specific marine regions tend to be relatively stable and are visually represented as alternating bright and dark stripes in SAR images. Thus, in regions prone to ISW occurrence, ISW feature confirmation was conducted based on two-dimensional NRCS images. If the features were unclear, other nearly synchronous optical or SAR images were matched to confirm the presence of ISWs.

This manuscript analyses the NRCS, SSHA, and SWH obtained from KaRIn and NALT. On the one hand, variations in sea surface roughness modulated by ISWs can alter electromagnetic wave propagation, affecting the NRCS. On the other hand, ISWs induce fluctuations in SSH during propagation, thereby altering the SSHA and SWH within the field of view. This phenomenon has been revealed by SRALs. For instance, Zhang et al. (2018b) utilized Sentinel-3 SRAL data and discovered that SSHA variations of approximately 50 cm were modulated by ISWs in the South China Sea. Magalhães and da Silva (2017) analyzed a total of 227 ISW data points using the Sentinel-3 SRAL and reported an average SSHA change of 40 cm modulated by ISWs.

3 ISWs observed by SWOT

3.1 *KaRIn*

A total of 14 datasets containing ISW features were screened in the South China Sea, Andaman Sea, Northeast Brazilian Sea, Sulu Sea, and Celes Sea. The results show that KaRIn has a breakthrough ability to detect mesoscale phenomena. It is capable of

Table 2. Interim Geophysical Data Record data product

Variables	Ku-band (1 Hz)	Ku-band (20 Hz)	C-band (1 Hz)	C-band (20 Hz)
NRCS	sig0_ocean_mle4 sig0_ocean_mle3 sig0_adaptive	sig0_ocean_mle4 sig0_ocean_mle3 sig0_adaptive sig0_ocog	sig0_ocean_mle4	sig0_ocean_mle4 sig0_ocog
SWH	swh_ocean_mle4 swh_ocean_mle3 swh_adaptive	swh_ocean_mle4 swh_ocean_mle3 swh_adaptive	swh_ocean_mle4	swh_ocean_mle4
SSHA	ssha_mle4 ssha_mle3	/	/	/

Note: / means the data under this condition is not available.

not only imaging sea surface features modulated by ISWs but also mapping two-dimensional sea surface height variation fields.

On November 3, 2023, at 12:17 (UTC+8), ISWs were detected in the northeastern Brazil. Figure 3a displays the KaRIn NRCS image, revealing multiple ISW wave packets moving northeast between 6°N and 9°N. This image not only displays large-scale crest wave features but also captures fine-scale details of the ISWs. These waves typically originate over the northeastern Brazilian continental shelf and then propagate northeastward into the Atlantic (Brandt et al., 2002; Magalhães et al., 2016). The dark-to-bright striped pattern in the image indicates descending-type ISWs, demonstrating the ability of KaRIn to reliably observe ISW sea surface features using SAR. However, due to observational constraints, the image did not cover the entire wave system and had a blank area of approximately 20 km in the nadir direction. To validate the detection ability of SWOT, other remote sensing images were collected. Figure 4a shows a Sentinel-3A Ocean and Land Colour Instrument (OLCI) image taken at 20:54 (UTC+8) on the same day, confirming that multiple ISW wave packets moved northeastward, which is consistent with the SWOT observations. This finding confirms the reliability of SWOT in detecting ISWs.

Figures 3b and c display L2 SSHA and L3 SSHA images detected by KaRIn. Compared with those of RAs and SRALs, the two-dimensional SSH field images of SWOT represent a revolutionary improvement. The stripe features corresponding to those in Figure 3a can be clearly recognized from the SSHA images. However, there were significant abnormalities in the L2 SSHA images. On the one hand, there was an imbalance in the fluctuation of heights between the left and right swaths, with the height variation in the left swath being negative and that in the right swath being positive. On the other hand, within each respective swath, the detection results from proximal to distal are also uneven. The discrepancies observed are attributed to inaccuracies in processing L2 data. Corrections are made using L3 level data, providing more accurate SSHA data. The results indicate that ISWs induce changes in the sea surface height field, with SSHA variations ranging from 15 cm to 25 cm at locations affected by ISW disturbances in the imagery. Additionally, Fig. 3d shows that the SWH image exhibits poor performance, failing to clearly depict the ISW characteristics or even discern the sea surface. This issue is attributed to its computational approach, which will be discussed in Section 4.

Figure 5 illustrates an instance detected on November 17, 2023, at 03:55 (UTC+8) in the Madagascar Island region. Within the NRCS image, multiple ISW packets of varying spatial scales are observed between 12°S and 8°S, primarily propagating northwest. These ISW patterns exhibit the characteristic alternation of dark and bright stripes, indicating hat they are descending ISWs. The SSHA images depicted in Figs 5b and c exhibit discernible

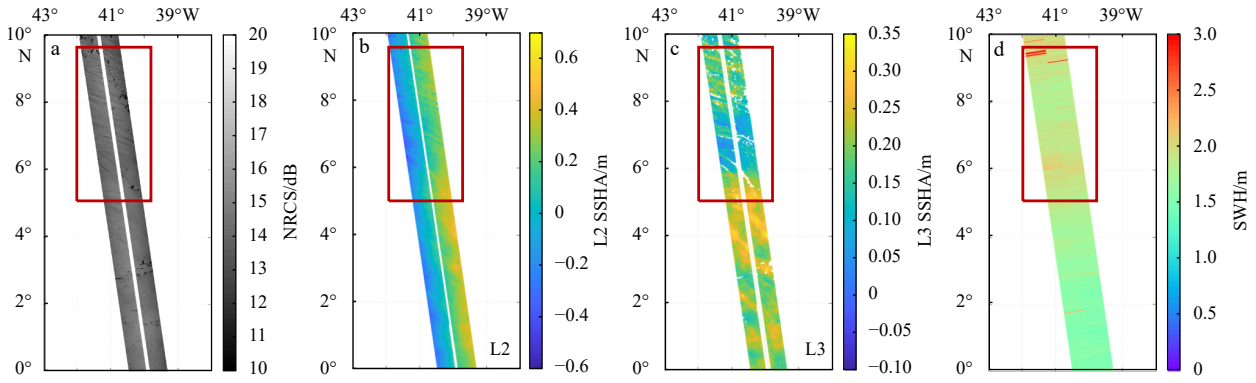

Fig. 3. Surface Water and Ocean Topography Ka-band radar interferometer images from November 3, 2023, in northeastern Brazil. a. Normalized radar cross section (NRCS), b. Level 2 (L2) sea surface height anomaly (SSHA), c. Level 3 (L3) SSHA, and d. significant wave height (SWH). The regions of internal solitary wave disturbance are marked by the red boxes.

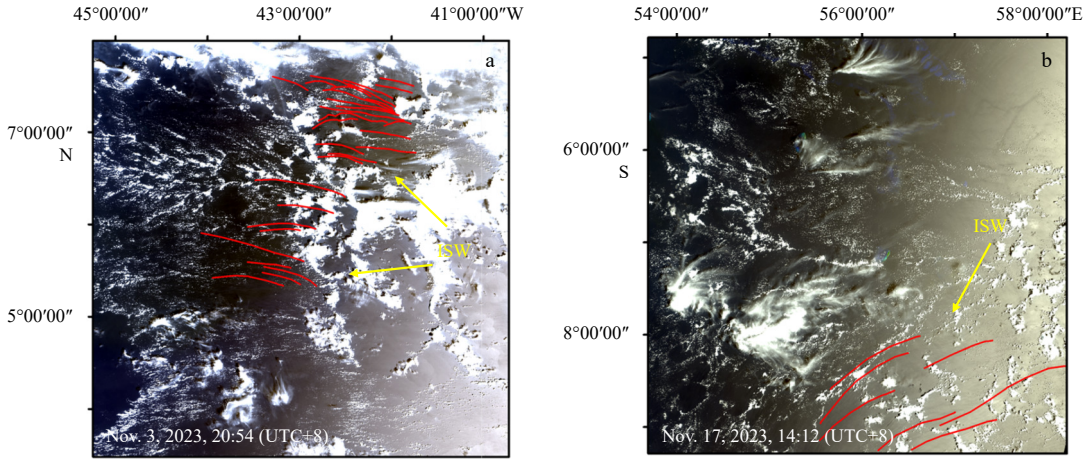

Fig. 4. The Sentinel-3 Ocean and Land Colour Instrument images. a. Northeast Brazil, corresponding to the data shown in Fig. 3. b. Northeastern Madagascar Island, corresponding to the data shown in Fig. 5. The red curves represent the crestlines of internal solitary waves.

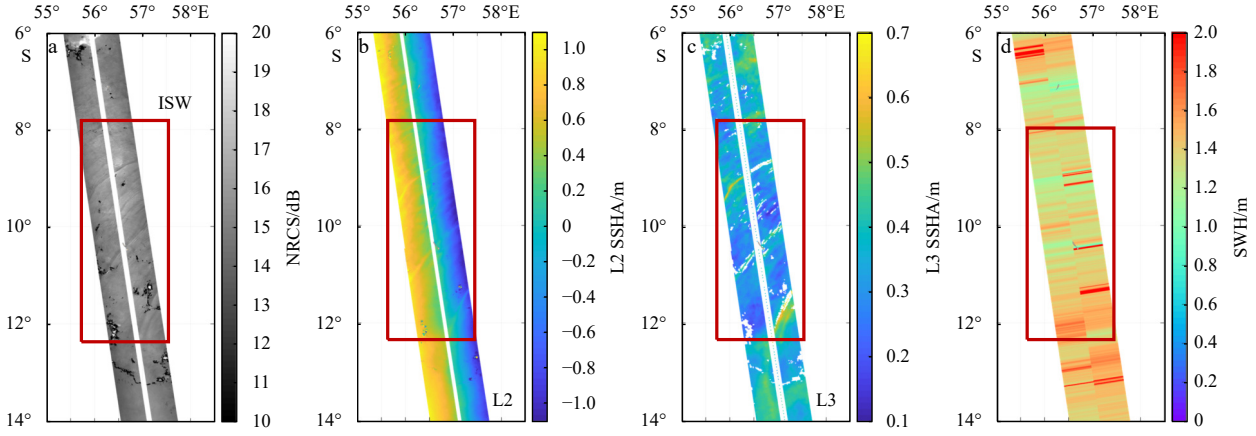

Fig. 5. Surface Water and Ocean Topography Ka-band radar interferometer images from November 16, 2023, near Madagascar Island. a. Normalized radar cross section (NRCS), b. Level 2 (L2) sea surface height anomaly (SSHA), c. Level 3 (L3) SSHA, and d. significant wave height (SWH). The regions of ISW disturbance are marked by the red boxes.

multiple crest lines of ISWs. Moreover, L2 SSHA images suffer from significant processing anomalies, notably an imbalance in sea surface height variations between the left and right stripes. Through L3 SSHA analysis, the modulating effect of these ISWs on the sea surface height field is notably pronounced, with SSHA variations reaching up to 60 cm at locations affected by ISW disturbances. Additionally, Fig. 5c, illustrating the L3 SSHA image, displays many missing values, especially in regions affected by ISW disturbances. This is attributed to the processing algorithm, which erroneously filters out larger SSHA variations modulated by ISWs as outliers. Consequently, the current analysis of L3 data underestimates the modulation of the sea surface height field by ISWs.

The Andaman Sea is a hotspot for studying ISWs and is characterized by large spatial scales but small wavelengths. The generation sources are diverse, and the propagation processes are complex, exhibiting evident wave-wave interactions. Hence, investigating ISW surface modulation with SWOT is a key focus, with the Andaman Sea being one of the priority areas. Figure 6 shows an image obtained on November 21, 2023, at 00:25 (UTC+8) in this region. In the NRCS image, numerous ISWs are visible across the entire sea area and are characterized by elongated wave crests but shorter wavelengths. However, in the SSHA image, the resolution of the ISW features is relatively weak, and short-wavelength solitons following crest lines are indiscernible. This indicates that the resolution of SWOT L2/L3 product data (2 km) is insufficient for the effective detection of ISWs with shorter wavelengths. The sea surface height variations induced by these ISWs are relatively small, less than 10 cm. At 07:19 (UTC+8), Sentinel-1A captured images of ISWs in the southern part of the Andaman Sea. Despite being approximately 7 hours after the SWOT observations, these images exhibited similar ISW characteristics. This is attributed to the relatively stable generation mechanism of ISWs in this region, resulting in similar features being elicited by adjacent tidal cycles.

3.2 *NALT*

The NALT carried out by SWOT operates in dual-frequency bands. The Ku-band provides high-precision height measurements, while the C-band offers high-precision wind speed measurements and ionospheric corrections. In this section, the ISW characteristics in profile data such as the NRCS, SWH, and SSHA

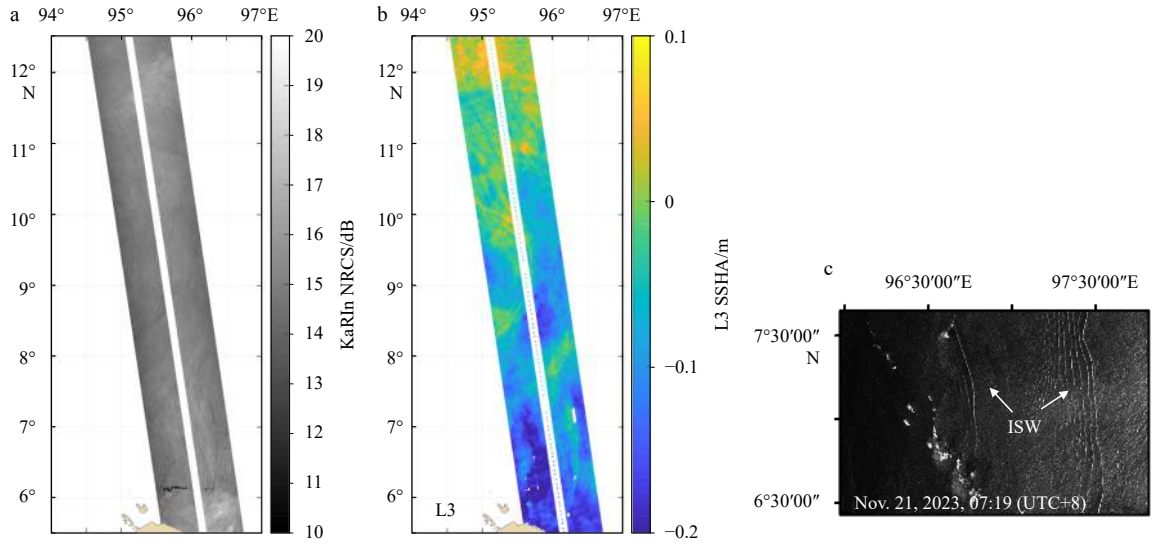

Fig. 6. Surface Water and Ocean Topography and Sentinel-1A images acquired in the Andaman Sea. a. Ka-band radar interferometer (KaRIn) normalized radar cross section (NRCS), b. Level 3 (L3) sea surface height anomaly (SSHA), and c. Sentinel-1A.

are analyzed based on 1 Hz and 20 Hz observational data. NALT employs various retracking algorithms, such as MLE4 (four-parameter maximum likelihood estimation) and MLE3 (three-parameter maximum likelihood estimation). This paper compares the results obtained from these algorithms. Notably, while NALT does not provide 20 Hz high-frequency SSHA data, interpolation can be applied for estimation.

On November 5, 2023, at 14:57 (UTC+8), and November 17, 2023, at 03:55 (UTC+8), SWOT passed through the Andaman Sea (Fig. 7a) and adjacent sea regions near Madagascar Island (Fig. 7b), where multiple packets of ISWs were detected. When analyzing ISW features in NALT data, it is essential to first identify the locations of ISW disturbances from KaRIn images. Based on the position information obtained from the KaRIn images, the perturbed regions can be isolated from the NALT observational data for further analysis. Subsequently, the detection results under different frequency bands, frequencies, and retracking methods can be compared and analyzed.

By analyzing the variations in the NRCS, we can investigate how changes in the sea surface height field induced by ISWs affect electromagnetic wave signals, as shown in Figs 8 and 9. During data processing, the impact of rainfall on signal attenuation must be considered. Rainfall effects are negligible when the liquid water content falls below 0.1 kg/m² (Magalhães and da Silva, 2017).

Affected by the modulation of ISWs, the NRCS increases from a steady state and then gradually returns to its initial level, indicating the distinct influence of ISWs on signal scattering. According to Figs 8a and 9a, Figs 8b and 9b, the measurements in the C-band exhibit a consistent bias higher than that in the Ku-band, approximately 1 dB. This discrepancy is related to the detection mechanisms of the two bands. A lower frequency of the C-band

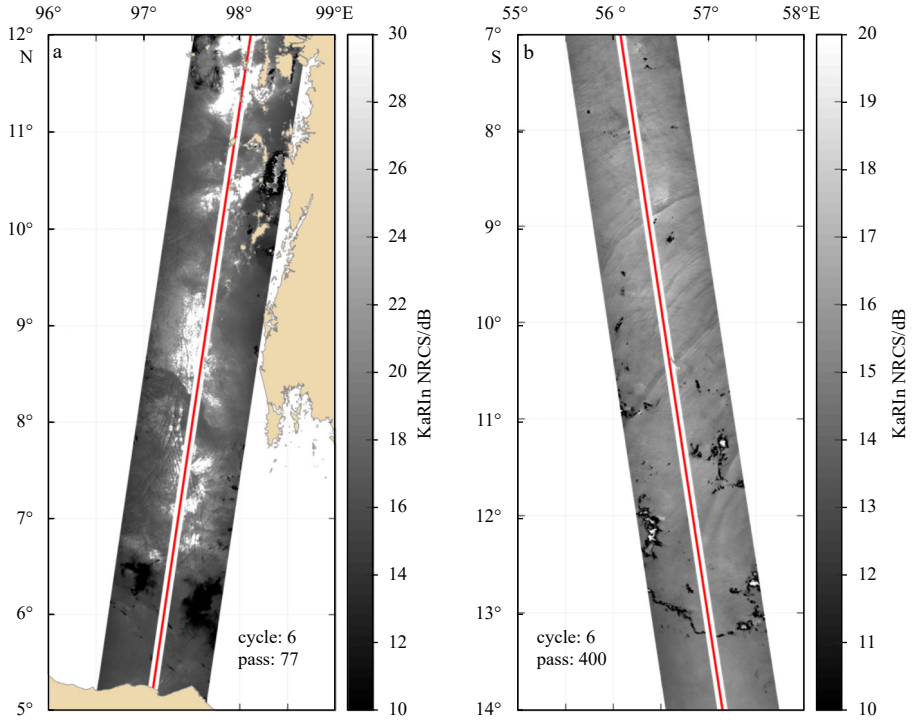

Fig. 7. Ka-band radar interferometer (KaRIn) normalized radar cross section (NRCS) images and Nadir altimeter trajectory. a. November 5, 2023, 14:57 (UTC+8), Andaman Sea. b. November 16, 2023, 03:55 (UTC+8), near Madagascar Island.

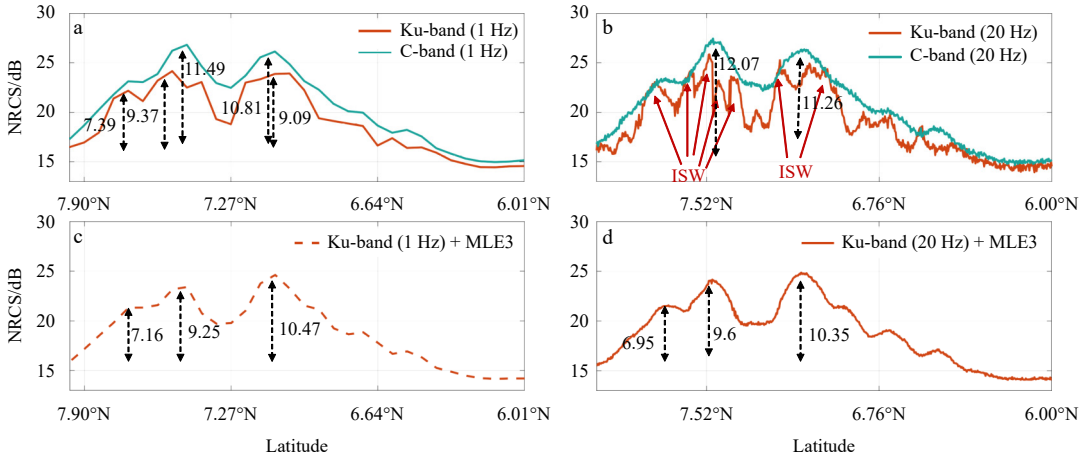

Fig. 8. Normalized radar cross section (NRCS) variations detected by Nadir altimeter, corresponding to Fig. 7a.

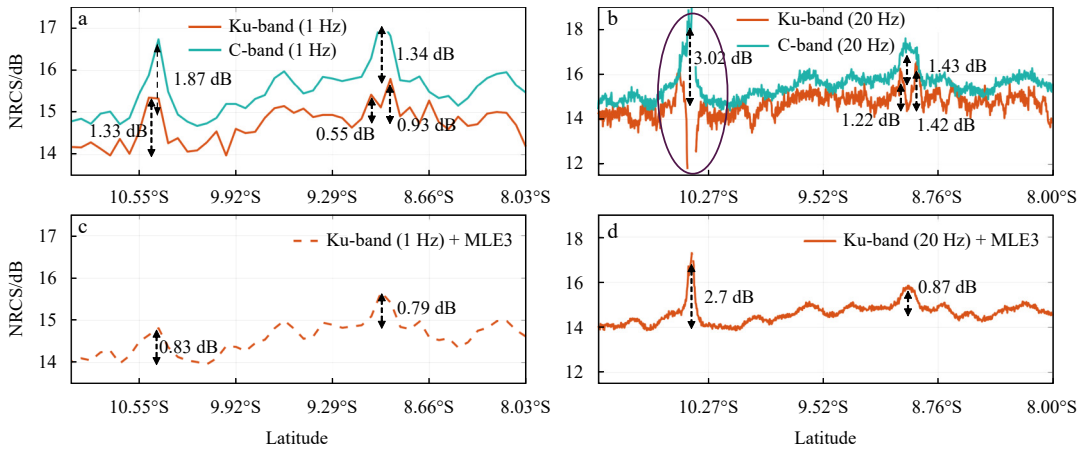

Fig. 9. Normalized radar cross section (NRCS) variations detected by Nadir altimeter, corresponding to Fig. 7b. Circle in b represents data anomaly due to internal solitary wave disturbances.

corresponds to shorter wavelengths, resulting in larger amplitude variations in the backscattered echoes caused by the same sea surface undulations. Additionally, C-band units typically have wider radiation angles, potentially receiving more scattered echoes from the sea surface under similar oceanic conditions, possibly leading to a systematic bias in the NRCSs toward higher values.

Moreover, the NRCS profiles in the C-band are broader and lack detailed features, whereas those in the Ku-band exhibit sharper profile changes, enabling better detection of detailed features. The detection results in the Ku-band exhibit the undulating structures of multiple ISWs, whereas in the C-band results, all undulating structures are merged into one, presenting a smoother appearance. This distinction arises from the shorter wavelength of the Ku-band, which is advantageous for detecting changes in small-scale surface waves. The modulation effect of ISWs on the ocean surface wave field primarily manifests in the convergence and divergence of fine-scale waves. This characteristic allows the Ku-band to more effectively capture and display the detailed features of ISWs.

The results obtained from the Ku-band using the MLE3 retracking method are presented in Figs 8c and 9c, Figs 8d and 9d. Compared to MLE4, the NRCS profiles obtained from MLE3 appear smoother but may lose some fine-grained details. MLE3 tends to favor smoother results. It typically assumes data stationarity during parameter estimation and favors the maximization of the likelihood function across the entire sequence, resulting in relatively smooth outputs (Thibaut et al., 2010). The primary objective of SWOT-carried NALT is to provide a reference value for KaRIn detection results, prioritizing the overall trend while disregarding minor fluctuations or noise. Conversely, MLE4 exhibits greater sensitivity to subtle variations in the data, increasing susceptibility to noise or outliers. Considering that ISWs generally manifest in packet-like forms and appear continuously in NALT footprints, MLE4 is more conducive to their detection. The figures illustrate the variations in the NRCSs attributed to ISWs, revealing a maximum change exceeding 10 dB and a minimum change of approximately 1 dB, indicating a large range of impacts on the NRCSs due to ISWs.

Figure 10 displays the NALT SWH variation profiles for the image shown in Fig. 7a. The results reveal anomalous SWH variations within the disturbed regions of ISWs in both frequency bands, with SWHs exceeding 10 m and even reaching up to 25 m. It is evident that such deviations significantly deviate from reality. The reason for this discrepancy lies in the interference caused by ISWs on the sea surface, affecting the processing of retracking algorithms and resulting in anomalously high SWH values. This issue has also been mentioned in the studies of Yu et al. (2022) and Magalhaes et al. (2023) using SRALs.

Figure 11 illustrates the SSHA profiles detected by the NALT.

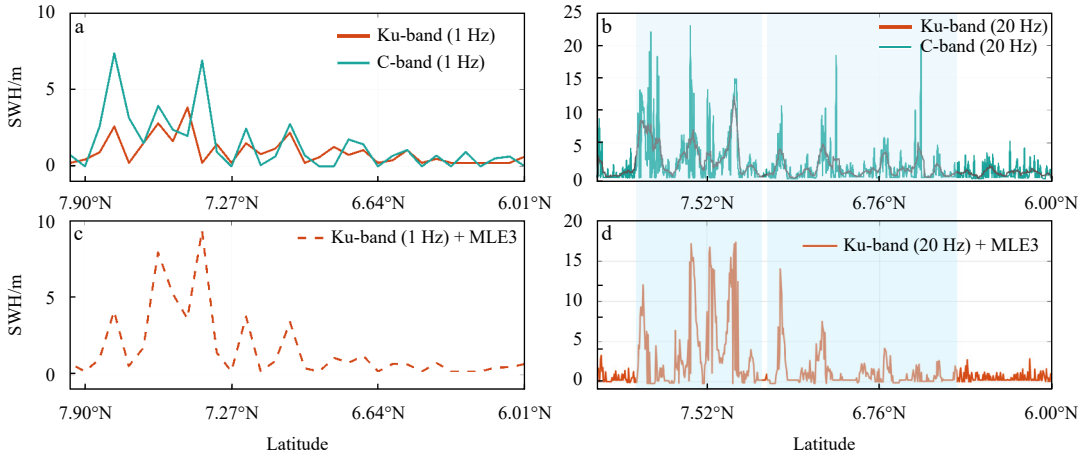

Fig. 10. Significant wave height (SWH) variations detected by Nadir altimeter, corresponding to Fig. 7a. Blue shaded areas represent the regions of internal solitary wave disturbance.

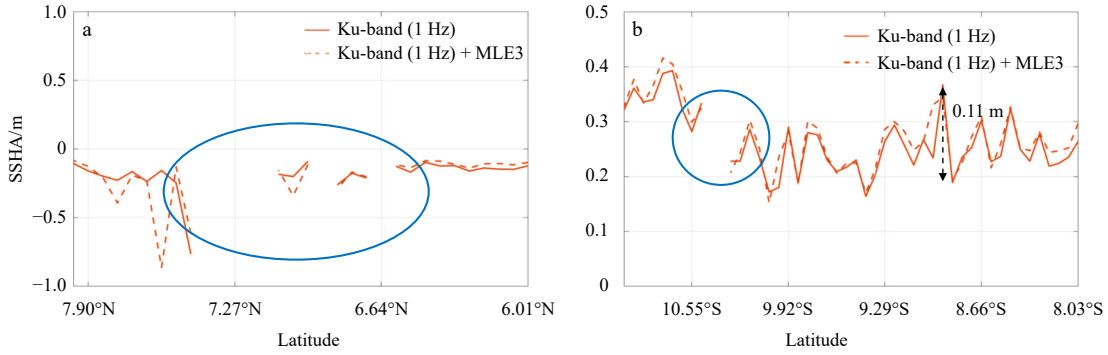

Fig. 11. The sea surface height anomaly (SSHA) variations detected by Nadir altimeter in the example shown in Fig. 7. Blue circles represent data anomalies due to internal solitary wave disturbances.

The blue circles in Fig. 11 denote anomalous issues, specifically the presence of numerous missing values (NaN) within the regions disturbed by ISWs. This problem resembles the SWH detection issue, where conventional altimeter retracking algorithms fail after these wave disturbances, resulting in significant anomalies in the computed results. However, SWOT's NALT primarily aims to provide reference values for KaRIn detection on both sides, and these abnormal values need to be removed. When investigating ISWs, recalculating the SSHA based on NALT measurements might still yield significant anomalies. Future research should explore how different surface structures of ISWs, such as convergence and divergence, affect altimeter echoes. This investigation could enhance the RA and SRAL detection processes and retracking algorithms concerning ISWs, thus improving SWH and SSHA calculations.

4 Discussion

Section 3 has demonstrated the detection capability of SWOT for ISWs, highlighting its outstanding advantages in terms of high resolution and wide swath imaging compared to RAs and SRALs. However, there are still some issues in the data analysis. First, although the swath width of SWOT KaRIn has been extended to 50 km on each side, it is still unable to cover the entire wave packet of ISWs, which typically have spatial scales of approximately 150 km.

Second, an issue arises in the SWH images in Fig. 3 to Fig. 5, where the discernibility is compromised. The SWH appears as blocky structures in the left and right swaths, and these structures are attributed to the processing algorithm of the imaging altimeter (Stiles Bryan, 2021). KaRIn receives radar signals from sea surface waves, converting them into the frequency domain. The integration of spectra within fixed spatial regions or swaths allows estimation of energy contributions for different wave heights, subsequently estimating SWH and filling these estimations across the entire swath. This results in blocky structures in the images, hindering the identification of ISWs and other oceanic processes. When large SWH variations exist within a swath, the overall computations tend to be biased more. For instance, in Figs 3d and 5d, the SWH near regions affected by ISW disturbances is notably overestimated due to their influence. Currently, there is no method available to address this issue; hence, the ability to utilize KaRIn SWH images for detecting ISWs is insufficient. Moreover, the asynchronous observations of SWOT's left and right bands result in the continuous propagation of ISWs, causing a noticeable displacement of crestlines between the two bands. Leveraging this trait, the propagation velocity of ISWs can be determined by calculating pixel distances and differences in imaging time.

Another noteworthy issue is the unevenness observed in the L2 SSHA images obtained by KaRIn, where there is an imbalance between the left and right swaths. The along-track SSHA profiles exhibit opposing trends with phase variation. This not only hampers the acquisition of reliable SSHA values but also results in the loss of detailed features within the images. This could be attributed to the ineffective removal of flat earth during interferometric phase processing by KaRIn. This paper optimized the processing of L2 SSHA data based on detrending principles. First, the trend component along the range direction of the SSHA profile was obtained and removed. Then, using the undisturbed sea surface as a reference, the relative variation in the SSHA was determined.

Figure 12 shows an image obtained near Dongsha Island on September 20, 2023, at 08:24 (UTC+8). The SWOT NRCS image reveals multiple spatially extensive wave packets with dense solitons, revealing ISWs in the left band that have traversed Dongsha Island, diverging from a single incident wave into two

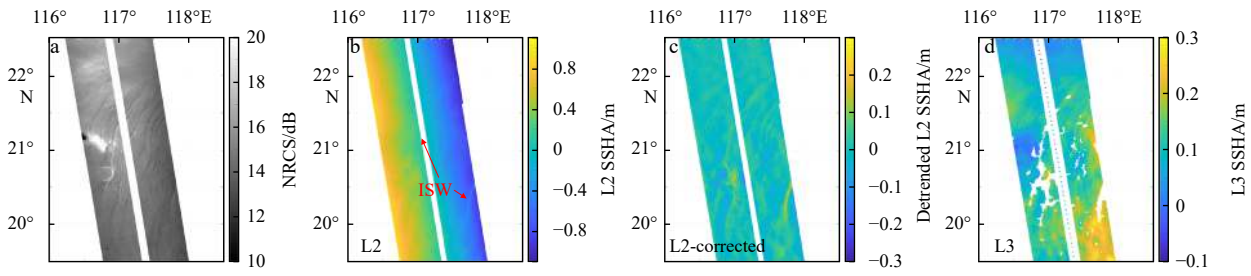

Fig. 12. Surface Water and Ocean Topography Ka-band radar interferometer images acquired on September 20, 2023, in the South China Sea. a. normalized radar cross section (NRCS), b. Level 2 (L2) sea surface height anomaly (SSHA), c. detrened L2 SSHA, and d. Level 3 (L3) SSHA.

refracted waves. Two hours later, both Moderate-resolution Imaging Spectroradiometer (MODIS) and Sentinel-2A captured images of ISWs in the region (Fig. 13), displaying features similar to those of the SWOT observations. However, Sentinel-2B, with its higher resolution, detected more detailed features of smaller solitons within the wave packets.

In the SSHA image in Fig. 12b, only the incident waves in the right band are discernible, with the subsequent details of solitons within the wave packets disappearing. A noticeable imbalance existed between the left and right bands, exhibiting opposing trends. Employing the method proposed for L2 SSHA image processing yielded the results shown in Fig. 12c. In comparison to the original data, the corrected SSHA no longer exhibited an imbalance between the left and right swaths, and the images showcased more features of ISWs. The SSHAs are generally elevated at the stripes of ISWs, indicating an increase in SSH in those regions. Figure 12d presents the L3 SSHA data the processing results obtained using the method proposed in this paper exhibit similar features, with comparable magnitudes of sea surface height variations. However, in the future, more suitable methods for correcting this phenomenon, such as interferometric processing of Level 1 (L1) data, should be considered. This approach can not only improve L2 data but also prevent the occurrence of missing SSHA values in regions disturbed by ISWs due to threshold settings in L3 data. Furthermore, despite the correction applied to the SSHA image revealing more features of ISWs, it still fails to identify ISWs with smaller wavelengths because of the resolution of approximately 2 km provided by SWOT KaRIn in its L2 product.

Based on SWOT KaRIn L3 SSHA data, quantitative statistical analysis was conducted on the sea surface height variations induced by ISWs. SSHA values were extracted along the crest lines of ISWs from the cases depicted in Figs 3, 5, 6, 12. Additionally, SSHA values from undisturbed calm sea surfaces were extracted. The results are presented in Fig. 14. The results indicate that in the four cases (all depicting descending-type ISWs), the SSHA

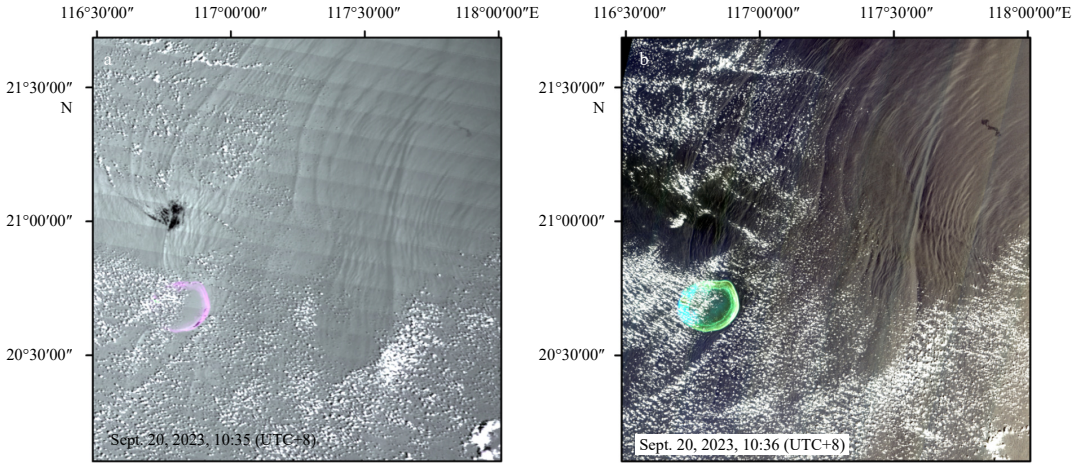

Fig. 13. Images were acquired on September 20, 2023, with the coordinate system being WGS1984. a. Moderate-resolution Imaging Spectroradiometer, 10:35 (UTC+8) and b. Sentinel-2B, 10:36 (UTC+8).

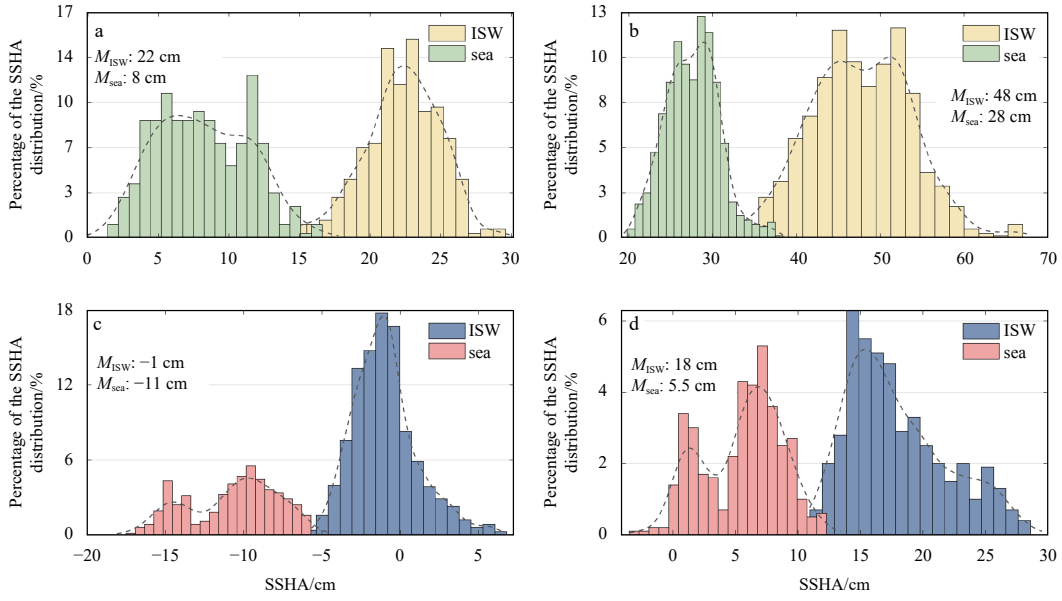

Fig. 14. Surface Water and Ocean Topography Ka-band radar interferometer Level 3 sea surface height anomaly (SSHA) statistical results corresponding to Fig. 3a, Fig. 5b, Fig. 6c, and Fig. 12d. The dashed lines represent the histogram fitting curves. ISW, internal solitary wave.

values at the locations disturbed by ISWs are greater than those of the surrounding sea surface, indicating a significant increase in sea surface height during propagation. Furthermore, the modulation of the sea surface height field by ISWs differs among the four examples, which is related to their amplitudes and water column stratification (Zhang et al., 2022). Taking the average values as a statistical reference, the modulation of the sea surface height field by ISWs increased by approximately 14 cm (175%), 20 cm (70%), 10 cm (90%), and 12.5 cm (220%) for the calm sea surfaces in each case.

5 Conclusions

SWOT is the latest generation of high-resolution, wide-swath imaging radar altimeters. It was launched on December 16, 2022, and its data were made publicly available in December 2023 after one year of on-orbit calibration. This paper analyses the sea surface height variations induced by ISWs using KaRIn and NALT onboard SWOT. Simultaneously, other remote sensing images were collected for synergistic validation with the SWOT detection results, further confirming the reliability of SWOT in detecting ISWs.

KaRIn has groundbreaking capabilities for detecting oceanic mesoscale phenomena, effectively imaging the surface features of ISWs, and mapping two-dimensional SSH changes. However, several issues still exist. First, the swath width of KaRIn cannot cover the entire ISW packet, thereby limiting observations. Second, the resolution of the L2/L3 level products provided by KaRIn is approximately 2 km, resulting in suboptimal performance in detecting smaller-scale ISWs due to their shorter wavelengths. Additionally, the SWH data display blocky structures within the two swaths, stemming from spectral integration processing algorithms. Currently, there is no optimized solution available to address this issue, consequently hindering the utilization of KaRIn's SWH data for ISW research.

In KaRIn L2 SSHA images, a notable systematic imbalance between the left and right swaths is evident, displaying opposing trends along the along-track profiles with phase variation tendencies. This imbalance results in unreliability in SSHA values and leads to the loss of significant detailed features within the images. This phenomenon might be linked to earlier flat earth effect removal processing methods. Detrending principles are employed to optimize this issue by processing the SSHA images after removing the trend component. This approach improved the identification of characteristics related to ISWs, and future investigations could delve deeper into analyzing and addressing this issue. An analysis of L3 data relvealed that descending-type ISWs cause an increase in the sea surface height field. In the four cases examined, the average SSHA modulation induced by ISWs ranges from 10 cm to 20 cm, with the maximum variation exceeding 200%.

The analysis of the capability of NALT to detect ISWs revealed that C-band measurements result in systematic overestimation, while Ku-band and MLE4 retracking are better suited for detecting these waves due to their greater sensitivity to minor variations in the data. However, in terms of SWH and SSHA, the data are largely unusable. This issue arises from the disturbance caused by ISWs on the sea surface, which impacts the processing of retracking algorithms and results in abnormally high amounts of data. Resolving this issue requires a deeper investigation into the influence of ISWs on sea surface structures, particularly their impact on altimeter echo signals. Tailored corrections are needed to enhance the retracking algorithms.

Undoubtedly, SWOT has demonstrated outstanding capabilities in detecting ISWs. Through extensive observational data, we can delve into the regulatory effects of ISWs on the sea surface, which are crucial for further comprehending their impact on ocean-atmosphere exchanges. Future research efforts should focus on refining the processing of SWOT data to extract ISW-related information more accurately and efficiently. This endeavor will aid in gaining deeper insights into the characteristics of ISWs and their influence on the marine environment.

Acknowledgements

Thanks to NASA and CNES for the publicly available SWOT NALT data and KaRIn low rate ocean products (https://www.aviso.altimetry.fr/en/missions/current-missions/swot/access-to-data.html).

References

Alpers W. 1985. Theory of radar imaging of internal waves. Nature, 314(6008): 245–247, doi: 10.1038/314245a0

Armitage T W K, Kwok R. 2021. SWOT and the ice-covered polar oceans: an exploratory analysis. Advances in Space Research, 68(2): 829–842, doi: 10.1016/j.asr.2019.07.006

Biancamaria S, Lettenmaier D P, Pavelsky T M. 2016. The SWOT mission and its capabilities for land hydrology. Surveys in Geophysics, 37(2): 307–337, doi: 10.1007/s10712-015-9346-y

Bole J B, Ebbesmeyer C C, Romea R D. 1994. Soliton currents in the South China Sea: measurements and theoretical modeling. In: Proceedings of the 26th Annual Offshore Technology Conference. Houston, Texas: OTC, OTC–7417-MS

Bondur V G, Serebryany A N, Zamshin V V. 2020. Registering fish shoals attracted by solitary intensive internal waves. Doklady Earth Sciences, 492(2): 471–474, doi: 10.1134/S1028334X20060033

Brandt P, Rubino A, Fischer J. 2002. Large-amplitude internal solitary waves in the North Equatorial Countercurrent. Journal of Physical Oceanography, 32(5): 1567–1573, doi: 10.1175/1520-0485(2002)032<1567:LAISWI>2.0.CO;2

Chaudhary A, Agarwal N, Sharma R, et al. 2021. Nadir altimetry Vis-à-Vis swath altimetry: a study in the context of SWOT mission for the Bay of Bengal. Remote Sensing of Environment, 252: 112120, doi: 10.1016/j.rse.2020.112120

da Silva J C B, Cerqueira A L F. 2016. A note on radar altimeter signatures of internal solitary waves in the ocean. In: Proceedings of SPIE 9999, Remote Sensing of the Ocean, Sea Ice, Coastal Waters, and Large Water Regions 2016. Edinburgh: SPIE, 999902

da Silva J C B, Santos-Ferreira A M, Rieu P, et al. 2020. Detection of internal solitary waves with conventional and advanced SAR altimetry processing methods: preliminary results. In: Proceedings of 2020 IEEE International Geoscience and Remote Sensing Symposium. Waikoloa: IEEE, 3521–3524

Dong Xiao, Zhang Yunhua, Zhai Wenshuai. 2017. Design and algorithms of the Tiangong-2 interferometric imaging radar altimeter processor. In: Proceedings of 2017 Progress in Electromagnetics Research Symposium. St. Petersburg: IEEE, 3802–3803

Donlon C, Berruti B, Buongiorno A, et al. 2012. The global monitoring for environment and security (GMES) Sentinel-3 mission. Remote Sensing of Environment, 120: 37–57, doi: 10.1016/j.rse.2011.07.024

Durand M, Fu L L, Lettenmaier D P, et al. 2010. The Surface Water and Ocean Topography Mission: observing terrestrial surface water and oceanic submesoscale eddies. Proceedings of the IEEE, 98(5): 766–779, doi: 10.1109/JPROC.2010.2043031

Fu L L, Alsdorf D, Rodriguez E, et al. 2009. The SWOT (Surface Water and Ocean Topography) mission: spaceborne radar interferometry for oceanographic and hydrological applications. In: Proceedings of the OCEANOBS'09 Conference. Venice, Italy: Sustained Ocean Observations and Informa- tion for Society

Fu L L, Ubelmann C. 2014. On the transition from profile altimeter to swath altimeter for observing global ocean surface topography.

Journal of Atmospheric and Oceanic Technology, 31(2): 560–568, doi: 10.1175/JTECH-D-13-00109.1

Gerkema T, Zimmerman J T F. 2008. An introduction to internal waves. Lecture Notes, Texel: Royal NIOZ, 207–208, https://docslib.org/doc/4371127/an-introduction-to-internal-waves [2023-12-12]

Gong Yankun, Xie Jieshuo, Xu Jiexin, et al. 2022. Oceanic internal solitary waves at the Indonesian submarine wreckage site. Acta Oceanologica Sinica, 41(3): 109–113, doi: 10.1007/s13131-021-1893-0

Huang Xiaodong, Chen Zhaohui, Zhao Wei, et al. 2016. An extreme internal solitary wave event observed in the northern South China Sea. Scientific Reports, 6(1): 30041, doi: 10.1038/srep30041

Jackson C R, da Silva J C B, Jeans G, et al. 2013. Nonlinear internal waves in synthetic aperture radar imagery. Oceanography, 26(2): 68–79

Le Traon P Y, Nadal F, Ducet N. 1998. An improved mapping method of multisatellite altimeter data. Journal of Atmospheric and Oceanic Technology, 15(2): 522–534, doi: 10.1175/1520-0426(1998)015<0522:AIMMOM>2.0.CO;2

Liu Yanliang, Putchim L, Li Kuiping, et al. 2022. Late monsoon threatens coral refugia in the Andaman Sea. Environmental Research Letters, 17(3): 034038, doi: 10.1088/1748-9326/ac4a30

Ma Zhimin, Han Guoqi. 2019. Reconstruction of the surface inshore Labrador current from SWOT sea surface height measurements. Remote Sensing, 11(11): 1264, doi: 10.3390/rs11111264

Magalhães J M, da Silva J C B. 2017. Satellite altimetry observations of large-scale internal solitary waves. IEEE Geoscience and Remote Sensing Letters, 14(4): 534–538, doi: 10.1109/LGRS.2017.2655621

Magalhães J M, da Silva J C B, Buijsman M C, et al. 2016. Effect of the North Equatorial Counter Current on the generation and propagation of internal solitary waves off the Amazon shelf (SAR observations). Ocean Science, 12(1): 243–255, doi: 10.5194/os-12-243-2016

Magalhaes J M, Lapa I G, Santos-Ferreira A M, et al. 2023. Using a tandem flight configuration between Sentinel-6 and Jason-3 to compare SAR and conventional altimeters in sea surface signatures of internal solitary waves. Remote Sensing, 15(2): 392, doi: 10.3390/rs15020392

Moore S E, Lien R C. 2007. Pilot whales follow internal solitary waves in the South China Sea. Marine Mammal Science, 23(1): 193–196, doi: 10.1111/j.1748-7692.2006.00086.x

Morrow R, Fu L L, Ardhuin F, et al. 2019. Global observations of fine-scale ocean surface topography with the Surface Water and Ocean Topography (SWOT) mission. Frontiers in Marine Science, 6: 232, doi: 10.3389/fmars.2019.00232

Nerem R S, Chambers D P, Choe C, et al. 2010. Estimating mean sea level change from the TOPEX and Jason altimeter missions. Marine Geodesy, 33(S1): 435–446

Pineda J, Rouse S, Starczak V, et al. 2020. Response of small sharks to nonlinear internal waves. Limnology and Oceanography, 65(4): 707–716, doi: 10.1002/lno.11341

Ray C, Martin-Puig C, Clarizia M P, et al. 2015. SAR altimeter backscattered waveform model. IEEE Transactions on Geoscience and Remote Sensing, 53(2): 911–919, doi: 10.1109/TGRS.2014.2330423

Santos-Ferreira A M, da Silva J C B. 2020. Can we retrieve internal soliton amplitudes in the ocean with SAR altimetry? What would this be good for?. In: Proceedings of 2020 IEEE International Geoscience and Remote Sensing Symposium. Waikoloa: IEEE, 3525–3528

Santos-Ferreira A M, da Silva J C B, Magalhaes J M. 2018. SAR mode altimetry observations of internal solitary waves in the tropical ocean Part 1: case studies. Remote Sensing, 10(4): 644, doi: 10.3390/rs10040644

Stammer D. 1997. Global characteristics of ocean variability estimated from regional TOPEX/POSEIDON altimeter measurements. Journal of Physical Oceanography, 27(8): 1743–1769, doi: 10.1175/1520-0485(1997)027<1743:GCOOVE>2.0.CO;2

Stiles Bryan W. 2021. KaRIn: ka-band radar interferometer on-board processor (OBP) algorithm theoretical basis document (ATBD). JPL D-79130. https://swot.jpl.nasa.gov/resources/documents/ [2021-03-08/2023-11-23]

Thibaut P, Poisson J C, Bronner E, et al. 2010. Relative performance of the MLE3 and MLE4 retracking algorithms on Jason-2 altimeter waveforms. Marine Geodesy, 33(S1): 317–335

Wang Yuhuai, Dai Changfeng, Chen Y Y. 2007. Physical and ecological processes of internal waves on an isolated reef ecosystem in the South China Sea. Geophysical Research Letters, 34(18): L18609

Yu Daocheng, Hwang C, Andersen O B, et al. 2021. Gravity recovery from SWOT altimetry using geoid height and geoid gradient. Remote Sensing of Environment, 265: 112650, doi: 10.1016/j.rse.2021.112650

Yu Changtian, Meng Junmin, Sun Lina, et al. 2022. Study of sea surface geophysical parameter changes due to internal solitary waves using a Sentinel-3 synthetic aperture radar altimeter. Remote Sensing, 14(21): 5375, doi: 10.3390/rs14215375

Zhang Hao, Fan Chenqing, Meng Junmin, et al. 2022. Research on internal solitary wave detection and analysis based on interferometric imaging radar altimeter onboard the Tiangong-2 space laboratory. Remote Sensing, 14(1): 174

Zhang Yunhua, Jiang Jingshan, Zhang Hongyuan, et al. 2000. Spaceborne imaging altimeter for topographic mapping. In: Proceedings of the IEEE 2000 International Geoscience and Remote Sensing Symposium. Taking the Pulse of the Planet: The Role of Remote Sensing in Managing the Environment. Proceedings (Cat. No.00CH37120). Honolulu: IEEE, 2349–2351

Zhang Yunhua, Shi Xiaojin, Wang Hongjian, et al. 2018a. Interferometric imaging radar altimeter on board Chinese Tiangong-2 space laboratory. In: Proceedings of 2018 Asia-Pacific Microwave Conference. Kyoto: IEEE, 851–853

Zhang Meng, Wang Jing, Li Zhixin, et al. 2022. Laboratory study of the impact of the surface solitary waves created by the internal solitary waves on optical imaging. Journal of Geophysical Research: Oceans, 127(2): e2021JC017800, doi: 10.1029/2021JC017800

Zhang Xudong, Zhang Jie, Fan Chenqing, et al. 2018b. Observations of internal waves with high sampling data of radar altimetry and MODIS images. International Journal of Remote Sensing, 39(21): 7405–7416, doi: 10.1080/01431161.2018.1470700

Zhang Xudong, Zhang Jie, Meng Junmin, et al. 2020. Observation of internal waves with OLCI and SRAL on board Sentinel-3. Acta Oceanologica Sinica, 39(3): 56–62, doi: 10.1007/s13131-019-1510-7